
CO Multi-line Imaging of Nearby Galaxies (COMING): I. Physical properties of molecular gas in the barred spiral galaxy NGC 2903

**Kazuyuki MURAOKA¹, Kazuo SORAI^{2,3}, Nario KUNO^{4,5}, Naomasa NAKAI^{4,5},
Hiroyuki NAKANISHI⁶, Miho TAKEDA¹, Kazuki YANAGITANI¹, Hiroyuki
KANEKO⁷, Yusuke MIYAMOTO⁷, Nozomi KISHIDA³, Takuya HATAKEYAMA⁴,
Michiko UMEI³, Takahiro TANAKA⁴, Yuto TOMIYASU⁴, Chey SAITA⁶, Saeko
UENO⁶, Naoko MATSUMOTO^{8,9}, Dragan SALAK¹⁰, and Kana
MOROKUMA-MATSUI⁹**

¹Department of Physical Science, Osaka Prefecture University, Gakuen 1-1, Sakai, Osaka
599-8531

²Department of Physics, Faculty of Science, Hokkaido University, Kita 10 Nishi 8, Kita-ku,
Sapporo 060-0810

³Department of Cosmosciences, Graduate School of Science, Hokkaido University, Kita 10
Nishi 8, Kita-ku, Sapporo 060-0810

⁴Division of Physics, Faculty of Pure and Applied Sciences, University of Tsukuba, 1-1-1
Tennodai, Tsukuba, Ibaraki 305-8571

⁵Center for Integrated Research in Fundamental Science and Technology (CiRfSE),
University of Tsukuba, Tsukuba, Ibaraki 305-8571

⁶Graduate School of Science and Engineering, Kagoshima University, 1-21-35 Korimoto,
Kagoshima, Kagoshima 890-0065

⁷Nobeyama Radio Observatory, Minamimaki, Minamisaku, Nagano 384-1305

⁸The Research Institute for Time Studies, Yamaguchi University, Yoshida 1677-1, Yamaguchi,
Yamaguchi 753-8511

⁹National Astronomical Observatory of Japan, 2-21-1 Osawa, Mitaka, Tokyo 181-8588

¹⁰Department of Physics, School of Science and Technology, Kwansai Gakuin University,

Abstract

We present simultaneous mappings of $J = 1 - 0$ emission of ^{12}CO , ^{13}CO , and C^{18}O molecules toward the whole disk ($8' \times 5'$ or $20.8 \text{ kpc} \times 13.0 \text{ kpc}$) of the nearby barred spiral galaxy NGC 2903 with the Nobeyama Radio Observatory 45-m telescope at an effective angular resolution of $20''$ (or 870 pc). We detected $^{12}\text{CO}(J = 1 - 0)$ emission over the disk of NGC 2903. In addition, significant $^{13}\text{CO}(J = 1 - 0)$ emission was found at the center and bar-ends, whereas we could not detect any significant $\text{C}^{18}\text{O}(J = 1 - 0)$ emission. In order to improve the signal-to-noise ratio of CO emission and to obtain accurate line ratios of $^{12}\text{CO}(J = 2 - 1)/^{12}\text{CO}(J = 1 - 0)$ ($R_{2-1/1-0}$) and $^{13}\text{CO}(J = 1 - 0)/^{12}\text{CO}(J = 1 - 0)$ ($R_{13/12}$), we performed the stacking analysis for our $^{12}\text{CO}(J = 1 - 0)$, $^{13}\text{CO}(J = 1 - 0)$, and archival $^{12}\text{CO}(J = 2 - 1)$ spectra with velocity-axis alignment in nine representative regions of NGC 2903. We successfully obtained the stacked spectra of the three CO lines, and could measure averaged $R_{2-1/1-0}$ and $R_{13/12}$ with high significance for all the regions. We found that both $R_{2-1/1-0}$ and $R_{13/12}$ differ according to the regions, which reflects the difference in the physical properties of molecular gas; i.e., density (n_{H_2}) and kinetic temperature (T_{K}). We determined n_{H_2} and T_{K} using $R_{2-1/1-0}$ and $R_{13/12}$ based on the large velocity gradient approximation. The derived n_{H_2} ranges from $\sim 1000 \text{ cm}^{-3}$ (in the bar, bar-ends, and spiral arms) to 3700 cm^{-3} (at the center) and the derived T_{K} ranges from 10 K (in the bar and spiral arms) to 30 K (at the center). We examined the dependence of star formation efficiencies (SFEs) on n_{H_2} and T_{K} , and found the positive correlation between SFE and n_{H_2} with the correlation coefficient for the least-square power-law fit R^2 of 0.50 . This suggests that molecular gas density governs the spatial variations in SFEs.

Key words: galaxies: ISM —galaxies: individual (NGC 2903) —galaxies: star formation

1 Introduction

Molecular gas is one of the essential components in galaxies because it is closely related to star formation, which is a fundamental process of galaxy evolution. Thus the observational study of molecular gas is indispensable to understand both star formation in galaxies and galaxy evolution.

However, the most abundant constituent in molecular gas, H_2 , cannot emit any electro-magnetic wave in cold molecular gas with typical temperature of ~ 10 K due to the lack of a permanent dipole moment. Instead, rotational transition lines of ^{12}CO , the second abundant molecule, have been used as a tracer of molecular gas. For example, some extensive ^{12}CO surveys of external galaxies, which consist of single pointings toward central regions and some mappings along the major axis, have been reported (e.g., Braine et al. 1993; Young et al. 1995; Elfhag et al. 1996). These studies provided new findings about global properties of galaxies, such as excitation condition of molecular gas in galaxy centers and radial distributions of molecular gas across galaxy disks.

In order to understand the relationship between molecular gas and star formation in galaxies further, spatially resolved ^{12}CO maps covering whole galaxy disks are necessary because star formation rates (SFRs) are often different between galaxy centers and disks. In particular, single-dish observations are essential to measure *total* molecular gas content in the observing beam from dense component to diffuse one avoiding the missing flux (e.g., Caldú-Primo et al. 2015). So far, two major surveys of wide-area ^{12}CO mapping toward nearby galaxies are performed using multi-beam receivers mounted on large single-dish telescopes.

One is the $^{12}\text{CO}(J = 1 - 0)$ mapping survey of 40 nearby spiral galaxies performed with the Nobeyama Radio Observatory (NRO) 45-m telescope in the position-switch mode (Kuno et al. 2007, hereafter K07). Their $^{12}\text{CO}(J = 1 - 0)$ maps cover most of the optical disks of galaxies at an angular resolution of $15''$, and clearly show two-dimensional distributions of molecular gas in galaxies. K07 found that the degree of the central concentration of molecular gas is higher in barred spiral galaxies than in non-barred spiral galaxies. In addition, they found a correlation between the degree of central concentration and the bar strength adopted from Laurikainen & Salo (2002)¹; i.e., galaxies with stronger bar tend to exhibit a higher central concentration. This correlation suggests that stronger bars accumulate molecular gas toward central regions more efficiently, which may contribute the onset of intense star formation at galaxy centers (i.e., higher SFRs than disks). Using the $^{12}\text{CO}(J = 1 - 0)$ data, Sorai et al. (2012) investigated the physical properties of molecular gas in the barred spiral galaxy Maffei 2. They found that molecular gas in the bar ridge regions may be gravitationally unbound, which suggests that molecular gas is hard to become dense, and to form stars in the bar.

The other survey is the Heterodyne Receiver Array CO Line Extragalactic Survey performed with the IRAM 30-m telescope (Leroy et al. 2009). They observed $^{12}\text{CO}(J = 2 - 1)$ emission over the full optical disks of 48 nearby galaxies at an angular resolution of $13''$, and found that the $^{12}\text{CO}(J = 2 - 1)/^{12}\text{CO}(J = 1 - 0)$ line intensity ratio (hereafter $R_{2-1/1-0}$) typically ranges from 0.6

¹ Laurikainen & Salo (2002) estimated the maxima of the tangential force and the averaged radial force at each radius in a bar using *JHK* band images, and they defined the maximum of the ratio between the two forces as the bar strength.

to 1.0 with the averaged value of 0.8. In addition, Leroy et al. (2013) examined a quantitative relationship between surface densities of molecular gas and SFRs for 30 nearby galaxies at a spatial resolution of 1 kpc using the $^{12}\text{CO}(J = 2 - 1)$ data. They found a first-order linear correspondence between surface densities of molecular gas and SFRs but also found second-order systematic variations; i.e., the apparent molecular gas depletion time, which is defined by the ratio of the surface density of molecular gas to that of SFR, becomes shorter with the decrease in stellar mass, metallicity, and dust-to-gas ratio. They suggest that this can be explained by a CO-to-H₂ conversion factor (X_{CO}) that depends on dust shielding.

However, such global CO maps of galaxies have raised a new question; the cause of the spatial variation in star formation efficiencies (SFEs) defined as SFRs per unit gas mass ². It is reported that SFEs differ not only among galaxies (e.g., Young et al. 1996) but also within locations/regions in a galaxy (e.g., Muraoka et al. 2007); i.e., higher SFEs are often observed in galaxy mergers rather than normal spiral galaxies and also observed in the nuclear star forming region rather than in galaxy disks. Some observational studies based on HCN emission, an excellent dense gas tracer, suggest that SFEs increase with the increase in molecular gas density (or dense gas fraction) in galaxies (e.g., Gao & Solomon 2004; Gao et al. 2007; Muraoka et al. 2009; Usero et al. 2015), but the cause of the spatial variation in SFEs is still an open question because HCN emission in galaxy disks is too weak to obtain its map except for some gas-rich spiral galaxies (e.g., M 51; Chen et al. 2015; Bigiel et al. 2016).

Instead, isotopes of CO molecule are promising probes of molecular gas density. In particular, $^{13}\text{CO}(J = 1 - 0)$ is thought to be optically thin and thus trace denser molecular gas ($\sim 10^{3-4}\text{cm}^{-3}$) rather than $^{12}\text{CO}(J = 1 - 0)$, which is optically thick and traces relatively diffuse molecular gas ($\sim 10^{2-3}\text{cm}^{-3}$). Therefore, the relative intensity between $^{13}\text{CO}(J = 1 - 0)$ and $^{12}\text{CO}(J = 1 - 0)$ is sensitive to physical properties of molecular gas. For example, spatial variations in $^{13}\text{CO}(J = 1 - 0)/^{12}\text{CO}(J = 1 - 0)$ intensity ratios (hereafter $R_{13/12}$) were observed in nearby galaxy disks (e.g., Sakamoto et al. 1997; Tosaki et al. 2002; Hirota et al. 2010). Such variations in $R_{13/12}$, typically ranging from 0.05 to 0.20, are interpreted as the variation in molecular gas density; i.e., $R_{13/12}$ increases with the increase in molecular gas density. However, some observations suggest that $R_{13/12}$ in central regions of nearby galaxies are lower than those in disk regions (e.g., Paglione et al. 2001; Tosaki et al. 2002; Hirota et al. 2010; Watanabe et al. 2011) although central regions of galaxies often show intense star formation activities, suggesting higher molecular gas density. The cause of the low $R_{13/12}$ in central regions is thought to be high temperature of molecular gas due to the heating by UV radiation from a lot of young massive stars.

Such a degeneracy between density and temperature of molecular gas in a line ratio can be

² In this paper, a correction factor to account for Helium and other heavy elements is not included in the calculation of molecular gas mass and SFE.

solved using two (or more) molecular line ratios with a theoretical calculation on the excitation of molecular gas such as the large velocity gradient (LVG) model (Scoville & Solomon 1974; Goldreich & Kwan 1974). For example, the density and kinetic temperature of giant molecular clouds (GMCs) were determined using $R_{13/12}$ and $^{12}\text{CO}(J = 3 - 2)/^{12}\text{CO}(J = 1 - 0)$ ratio for Large Magellanic Cloud (Minamidani et al. 2008) and M 33 (Muraoka et al. 2012), and also determined using $R_{13/12}$ and $R_{2-1/1-0}$ for the spiral arm of M 51 (Schinnerer et al. 2010). This method to determine molecular gas density is useful to investigate the cause of the variation in SFEs. Thus the dependence of SFEs on molecular gas density should be investigated for various galaxies at high angular resolution based on multiple line ratios including $R_{13/12}$.

In this paper, we investigate the relationship between SFE and molecular gas density within a nearby barred spiral galaxy NGC 2903 using an archival $^{12}\text{CO}(J = 2 - 1)$ map combined with $^{12}\text{CO}(J = 1 - 0)$ and $^{13}\text{CO}(J = 1 - 0)$ maps which are newly obtained by the CO Multi-line Imaging of Nearby Galaxies (COMING) project with the NRO 45-m telescope. NGC 2903 is a gas-rich galaxy exhibiting bright nuclear star formation (e.g., Wynn-Williams & Becklin 1985; Simons et al. 1988; Alonso-Herrero et al. 2001; Yukita et al. 2012). The distance to NGC 2903 is estimated to be 8.9 Mpc (Drozdovsky & Karachentsev 2000); thus the effective angular resolution of $20''$ for the on-the-fly (OTF) mapping with the NRO 45-m corresponds to 870 pc. This enables us to resolve major structures within NGC 2903, such as the center, bar, and spiral arms although its inclination of 65° (de Blok et al. 2008) is not so small. In addition, NGC 2903 is rich in archival multi-wavelength data set; i.e., not only the $^{12}\text{CO}(J = 2 - 1)$ map to examine $R_{2-1/1-0}$ but also $\text{H}\alpha$ and infrared images to calculate SFRs are available. Thus this galaxy is a preferable target to examine the cause of the variation in SFE in terms of molecular gas density. Basic parameters of NGC 2903 are summarized in table 1.

The structure of this paper is as follows: We describe the overview of the COMING project and explain the detail of the CO observations and data reduction for NGC 2903 in section 2. Then, we show results of observations; i.e., spectra and velocity-integrated intensity maps of $^{12}\text{CO}(J = 1 - 0)$ and $^{13}\text{CO}(J = 1 - 0)$ emission in section 3. We obtain averaged spectra of $^{12}\text{CO}(J = 1 - 0)$, $^{13}\text{CO}(J = 1 - 0)$, and $^{12}\text{CO}(J = 2 - 1)$ emission for nine representative regions, and measure averaged $R_{13/12}$ and $R_{2-1/1-0}$ for each region in section 4.1. We determine molecular gas density and kinetic temperature for the center, bar, bar-ends, and spiral arms using $R_{13/12}$ and $R_{2-1/1-0}$ based on the LVG approximation in section 4.2. Finally, we investigate the cause of the variation in SFE by examining the dependence of SFE on molecular gas density and kinetic temperature.

2 Observations and data reduction

2.1 COMING project

COMING is a project to map $J = 1 - 0$ emission of ^{12}CO , ^{13}CO , and C^{18}O molecules simultaneously for 70% area of optical disks of 238 galaxies using the FOur-beam REceiver System on 45-m Telescope (FOREST; Minamidani et al. 2016) at NRO. The main purposes of the COMING are to characterize properties of molecular gas as sequence of, Hubble types, dynamical structures, central concentrations, and star formation activities, as well as surrounding environments of galaxies. More detailed information on COMING project including the current status of the survey will be reported in the forthcoming paper (Sorai et al. in preparation).

2.2 Observations

$^{12}\text{CO}(J = 1 - 0)$, $^{13}\text{CO}(J = 1 - 0)$, and $\text{C}^{18}\text{O}(J = 1 - 0)$ emission observations of NGC 2903 were performed using the NRO 45-m telescope from April to May, 2015, employing the OTF mapping mode. The observed area is about $8' \times 5'$, which corresponds to 20.8×13.0 kpc at the distance of 8.9 Mpc, as indicated in figure 1. The total time for the observations was 13 hrs.

We used a new 2×2 focal-plane dual-polarization sideband-separating SIS mixer receiver for the single side band (SSB) operation, FOREST, which provides 8 intermediate frequency (IF) paths (i.e., 4 beam \times 2 polarization) independently. Owing to the wide IF range of 4 to 12 GHz, we could simultaneously observe $^{12}\text{CO}(J = 1 - 0)$ emission at 115 GHz (IF = 10 GHz) and $^{13}\text{CO}(J = 1 - 0)$ and $\text{C}^{18}\text{O}(J = 1 - 0)$ emission at 110 GHz (IF = 5 GHz) when the frequency of the local oscillator was set to 105 GHz. The backend was an FX-type correlator system, SAM45, which consists of 16 arrays with 4096 spectral channels each. We set the frequency coverage and resolution for each array of 2 GHz and 488.24 kHz, which gives velocity coverage and resolution of 5220 km s^{-1} and 1.27 km s^{-1} at 115 GHz, and those of 5450 km s^{-1} and 1.33 km s^{-1} at 110 GHz. We assigned 8 of 16 arrays to 115 GHz band (i.e., IF = 9 – 11 GHz for $^{12}\text{CO}(J = 1 - 0)$ emission) and other 8 arrays to 110 GHz band (i.e., IF = 4 – 6 GHz for $^{13}\text{CO}(J = 1 - 0)$ and $\text{C}^{18}\text{O}(J = 1 - 0)$ emission). The half-power beam widths of the 45-m with the FOREST were $\sim 14''$ at 115 GHz and $\sim 15''$ at 110 GHz, respectively. The system noise temperatures were 300 – 500 K at 115 GHz and 200 – 250 K at 110 GHz during the observing run.

We performed the OTF mapping along the major and minor axes of the galaxy disk whose position angle was 25° (K07). The separation between the scan rows was set to $5.''0$, and the spatial sampling interval was $< 2.''4$ applying a dump time of 0.1 second and a scanning speed of $< 24'' \text{ s}^{-1}$. The data sets scanned along two orthogonal axes were co-added by the Basket-weave method (Emerson

& Graeve 1988) to remove any effects of scanning noise. In order to check the absolute pointing accuracy every hour, we observed an SiO maser source, W-Cnc, using a 43 GHz band receiver. It was better than $6''$ (peak-to-peak) throughout the observations. In addition, we observed $^{12}\text{CO}(J = 1 - 0)$ and $^{13}\text{CO}(J = 1 - 0)$ emission of W 3 and IRC+10216 every day to obtain the scaling factors for converting the observed antenna temperature to the main beam temperature for each IF. Note that these scaling factors not only correct the main-beam efficiency (η_{MB}) of the 45-m antenna but also compensate the decrease in line intensity due to the incompleteness of the image rejection for SSB receiver (e.g., Nakajima et al. 2013). The absolute error of the temperature scale for each CO spectrum was about $\pm 20\%$, mainly due to variations in η_{MB} and the image rejection ratio of the FOREST.

2.3 Data reduction

Data reduction was made using the software package NOSTAR, which comprises tools for OTF data analysis, developed by NRO (Sawada et al. 2008). We excluded bad spectra, which includes strong baseline undulation and spurious lines, from the raw data. Then, linear baselines were subtracted, and the raw data were regridded to $6''$ per pixel with an effective angular resolution of approximately $20''$ (or 870 pc). We binned the adjacent spectral channels to a velocity resolution of 10 km s^{-1} for the spectra. Finally, we created three-dimensional data cubes in $^{12}\text{CO}(J = 1 - 0)$, $^{13}\text{CO}(J = 1 - 0)$, and $\text{C}^{18}\text{O}(J = 1 - 0)$ emission. The resultant r.m.s. noise levels (1σ) were 60 mK, 39 mK, and 40 mK for $^{12}\text{CO}(J = 1 - 0)$, $^{13}\text{CO}(J = 1 - 0)$, and $\text{C}^{18}\text{O}(J = 1 - 0)$, respectively.

3 Results

3.1 $^{12}\text{CO}(J = 1 - 0)$ emission

Figure 2 shows $^{12}\text{CO}(J = 1 - 0)$ spectra of the whole optical disk in NGC 2903. As is the case in earlier studies (e.g., Helfer et al. 2003, K07, Leroy et al. 2009), strong $^{12}\text{CO}(J = 1 - 0)$ emission, whose peak temperature was $\sim 0.6 \text{ K}$, was found at the center and significant $^{12}\text{CO}(J = 1 - 0)$ emission was detected in the bar ($\sim 0.3 \text{ K}$), bar-ends ($0.4 - 0.5 \text{ K}$), and spiral arms ($0.1 - 0.3 \text{ K}$).

We calculate velocity-integrated $^{12}\text{CO}(J = 1 - 0)$ intensities ($I_{^{12}\text{CO}(1-0)}$) from the spectra. In order to obtain more accurate line intensities (in other words, to minimize the effects of the noise and the undulation of baseline for weak line), we defined the “line channels”, which are successive velocity channels where significant emission exists, in advance for each pixel as described below.

In order to define the “line channels”, we utilized $^{12}\text{CO}(J = 2 - 1)$ data (Leroy et al. 2009), which was regridded and convolved to $20''$ to match our $^{12}\text{CO}(J = 1 - 0)$ spectra. Since the 1σ r.m.s. of $^{12}\text{CO}(J = 2 - 1)$ data of 6 mK at $20''$ and 10 km s^{-1} resolutions was 10 times better than that of our

$^{12}\text{CO}(J = 1 - 0)$ data, the $^{12}\text{CO}(J = 2 - 1)$ spectra are appropriate for the decision of “line channels” in each pixel. We first identified a velocity channel exhibiting the peak $^{12}\text{CO}(J = 2 - 1)$ temperature and defined the channel as the “CO peak channel” for each pixel. Then, successive channels whose $^{12}\text{CO}(J = 2 - 1)$ emission consistently exceeds 1σ including the “CO peak channel” are defined as “line channels”. Finally, we calculated $I_{12\text{CO}(1-0)}$ for the specified “line channels” in each pixel.

Figure 3 shows the $I_{12\text{CO}(1-0)}$ map of NGC 2903. The strongest $I_{12\text{CO}(1-0)}$ of 92 K km s^{-1} is observed at the center, and the secondary peak of 55 K km s^{-1} is at the northern bar-end. The total molecular gas mass for the observed area in NGC 2903 is estimated to $(2.8 \pm 0.6) \times 10^9 M_{\odot}$ under the assumptions of the constant X_{CO} of $1.8 \times 10^{20} \text{ cm}^{-2} (\text{K km s}^{-1})^{-1}$ (Dame et al. 2001) over the disk and the uncertainty of 20% in brightness temperature scape of CO line. This value is consistent with $3.2 \times 10^9 M_{\odot}$ obtained by K07, which is recalculated using the same distance and X_{CO} . We also compare $I_{12\text{CO}(1-0)}$ obtained by COMING with those obtained by K07 to confirm the validity of our $^{12}\text{CO}(J = 1 - 0)$ data. We examined the pixel-by-pixel comparison for the two $I_{12\text{CO}(1-0)}$ maps at the same angular resolution of $20''$ as shown in figure 4, and confirmed that both $I_{12\text{CO}(1-0)}$ are well correlated with each other. The median and the standard deviation in $I_{12\text{CO}(1-0)}$ are 12.9 K km s^{-1} and 12.4 K km s^{-1} for COMING dataset, and those are 15.2 K km s^{-1} and 12.6 K km s^{-1} for K07 dataset.

3.2 $^{13}\text{CO}(J = 1 - 0)$ and $\text{C}^{18}\text{O}(J = 1 - 0)$ emission

Figure 5(a) shows the global $^{13}\text{CO}(J = 1 - 0)$ spectra, which are overlaid by $^{12}\text{CO}(J = 1 - 0)$ spectra for comparison. In addition, figure 5(b), (c), and (d) show the magnified $^{13}\text{CO}(J = 1 - 0)$ spectra at the northern bar-end, the center, and the southern bar-end, respectively. We found significant $^{13}\text{CO}(J = 1 - 0)$ emission at the center and both bar-ends. However, we could not detect any significant $\text{C}^{18}\text{O}(J = 1 - 0)$ emission.

We calculated the velocity-integrated $^{13}\text{CO}(J = 1 - 0)$ intensities ($I_{13\text{CO}(1-0)}$). As is the case of $^{12}\text{CO}(J = 1 - 0)$, we utilized the “line channels” defined by $^{12}\text{CO}(J = 2 - 1)$ spectra. Figure 6 shows a spatial distribution of $I_{13\text{CO}(1-0)}$ in pseudo-color overlaid by $I_{12\text{CO}(1-0)}$ in contour. The global distribution of $^{13}\text{CO}(J = 1 - 0)$ is similar to $^{12}\text{CO}(J = 1 - 0)$; several peaks whose $I_{13\text{CO}(1-0)}$ exceeds 5 K km s^{-1} are observed at the center, bar-ends, and in spiral arms.

3.3 Line intensity ratios $R_{2-1/1-0}$ and $R_{13/12}$

Intensity ratios of two (or more) molecular lines provide important clues to estimate physical properties of molecular gas, such as density and temperature. We examined the spatial variations in line

intensity ratios among $^{12}\text{CO}(J = 1 - 0)$, $^{13}\text{CO}(J = 1 - 0)$, and $^{12}\text{CO}(J = 2 - 1)$ emission. Figure 7 shows spatial distributions of $R_{2-1/1-0}$ and $R_{13/12}$ over the disk of NGC 2903. In these maps, we displayed pixels with each line intensity exceeding 2σ (5 K km s^{-1} , 3 K km s^{-1} , and 0.5 K km s^{-1} for $^{12}\text{CO}(J = 1 - 0)$, $^{13}\text{CO}(J = 1 - 0)$, and $^{12}\text{CO}(J = 2 - 1)$, respectively). We found some local peaks of $R_{2-1/1-0}$ (~ 1.0) near the center and at the downstream side of the northern spiral arm, whereas lower $R_{2-1/1-0}$ ($\sim 0.5 - 0.6$) was observed in the bar. The spatial distribution of $R_{13/12}$ is unclear due to poor signal-to-noise (S/N) ratio of $^{13}\text{CO}(J = 1 - 0)$ emission.

4 Discussion

4.1 Velocity-axis alignment stacking of CO spectra

As described in section 3.3, the spatial distribution of $R_{13/12}$ seems noisy and unclear due to the poor S/N although we could obtain the spatial distribution of $I_{13\text{CO}(1-0)}$. In order to improve the S/N of weak emission such as $^{13}\text{CO}(J = 1 - 0)$, the stacking analysis of CO spectra with the velocity-axis alignment seems a promising method.

The stacking technique for CO spectra in external galaxies are originally demonstrated by Schruba et al. (2011, 2012). Since the observed velocities of each position within a galaxy are different due to its rotation, a simple stacking causes a smearing of spectrum. In order to overcome such difficulty, Schruba et al. (2011) demonstrated the velocity-axis alignment of CO spectra in different regions in a galaxy disk according to mean HI velocity. They stacked velocity-axis aligned CO spectra, and successfully confirmed very weak $^{12}\text{CO}(J = 2 - 1)$ emission ($< 1\text{ K km s}^{-1}$) with high significance in HI-dominated outer-disk regions of nearby spiral galaxies. In addition, Schruba et al. (2012) applied this stacking technique to perform the sensitive search for weak $^{12}\text{CO}(J = 2 - 1)$ emission in dwarf galaxies. Furthermore, Morokuma-Matsui et al. (2015) applied the stacking technique to $^{13}\text{CO}(J = 1 - 0)$ emission in the optical disk of the nearby barred spiral galaxy NGC 3627. By the stacking with velocity-axis alignment based on mean $^{12}\text{CO}(J = 1 - 0)$ velocity, they obtained high S/N $^{13}\text{CO}(J = 1 - 0)$ spectra which are improved by a factor of up to 3.2 compared to the normal (without velocity-axis alignment) stacking analysis.

These earlier studies clearly suggest that the stacking analysis is very useful to detect weak molecular line. In this section, we employ the same stacking technique as Morokuma-Matsui et al. (2015) to improve the S/N of $^{13}\text{CO}(J = 1 - 0)$ emission and to obtain more accurate line ratios. Based on our $I_{12\text{CO}(1-0)}$ image (figure 3), we have separated NGC 2903 into nine regions according to its major structures; i.e., center, northern bar, southern bar, northern bar-end, southern bar-end, northern arm, southern arm, inter-arm, and outer-disk. The left panel of figure 8 shows the separation of each

region overlaid by the grey-scale map of $I_{12\text{CO}(1-0)}$. For each region, we stacked $^{12}\text{CO}(J = 1 - 0)$, $^{13}\text{CO}(J = 1 - 0)$, and $^{12}\text{CO}(J = 2 - 1)$ spectra with velocity-axis alignment based on the intensity-weighted mean velocity field calculated from our $^{12}\text{CO}(J = 1 - 0)$ data (right panel of figure 8). We successfully obtained the stacked CO spectra as shown in figure 9. The S/N of each CO emission is dramatically improved, and thus we could confirm the significant $^{13}\text{CO}(J = 1 - 0)$ emission for all the regions. We found the difference in the line shape of stacked CO spectra according to regions. In particular, the stacked ^{12}CO spectra in the bar show flat peak over the velocity width of 100 – 150 km s⁻¹. This is presumably due to the rapid velocity change in the bar, which makes the velocity-axis alignment difficult.

We summarize the averaged line intensities and line ratios for each region in table 2. We found that the averaged $R_{2-1/1-0}$ shows the highest value of 0.92 at the center, and a moderate value of 0.7 – 0.8 at both bar-ends and in the northern arm. A slightly lower $R_{2-1/1-0}$ of 0.6 – 0.7 is observed in the bar, southern arm, inter-arm, and outer-disk. Such a variation in $R_{2-1/1-0}$ ranging from 0.6 to 1.0 in NGC 2903 is quite consistent with those observed in nearby galaxies (e.g., Leroy et al. 2009). However, the highest $R_{13/12}$ of 0.19 is observed not at the center but in the northern arm. The central $R_{13/12}$ of 0.11 is similar to those in other regions (0.08 – 0.13) except for the northern arm and outer-disk (~ 0.04). The typical $R_{13/12}$ of ~ 0.1 is frequently observed in nearby galaxies (e.g., Paglione et al. 2001; Vila-Vilaro et al. 2015), but slightly higher than the averaged $R_{13/12}$ in representative regions of NGC 3627, 0.04 – 0.09 (Morokuma-Matsui et al. 2015).

4.2 Derivation of physical properties and their comparison with star formation

4.2.1 LVG calculation for stacked CO spectra

Using $R_{2-1/1-0}$ and $R_{13/12}$, we derive averaged physical properties of molecular gas, its density (n_{H_2}) and kinetic temperature (T_{K}), in seven regions (center, northern bar, southern bar, northern bar-end, southern bar-end, northern arm, and southern arm) of NGC 2903 based on the LVG approximation. Some assumptions are required to perform the LVG calculation; the molecular abundances $Z(^{12}\text{CO}) = [^{12}\text{CO}]/[\text{H}_2]$, $[^{12}\text{CO}]/[^{13}\text{CO}]$, and the velocity gradient dv/dr . Firstly, we fix the $Z(^{12}\text{CO})$ of 1.0×10^{-5} and dv/dr of $1.0 \text{ km s}^{-1} \text{ pc}^{-1}$; i.e., ^{12}CO abundance per unit velocity gradient $Z(^{12}\text{CO})/(dv/dr)$ was assumed to $1.0 \times 10^{-5} (\text{km s}^{-1} \text{ pc}^{-1})^{-1}$. This is the same as the assumed $Z(^{12}\text{CO})/(dv/dr)$ for GMCs in M 33 (Muraoka et al. 2012).

Then, we determine the $[^{12}\text{CO}]/[^{13}\text{CO}]$ abundance ratio to be assumed in this study by considering earlier studies. Langer & Penzias (1990) found a systematic gradient in the $^{12}\text{C}/^{13}\text{C}$ isotopic ratio across in our Galaxy; from ~ 30 in the inner part at 5 kpc to ~ 70 at 12 kpc with a galactic center

value of 24. For external galaxies, the reported $^{12}\text{C}/^{13}\text{C}$ isotopic ratios in their central regions are 40 for NGC 253 (Henkel et al. 1993), 50 for NGC 4945 (Henkel et al. 1994), > 40 for M 82 and > 30 for IC 342 (Henkel et al. 1998). Mao et al. (2000) reported a higher $^{12}\text{CO}/^{13}\text{CO}$ abundance ratio of 50 – 75 in the central region of M 82. Martín et al. (2010) also reported a higher $^{12}\text{C}/^{13}\text{C}$ isotopic ratios of > 50 – 100 in the central regions of M 82 and NGC 253. In summary, reported $^{12}\text{C}/^{13}\text{C}$ isotopic (and $^{12}\text{CO}/^{13}\text{CO}$ abundance) ratios in nearby galaxy centers (30 – 100) are typically higher than that in the inner 5 kpc of our Galaxy (24 – 30), but the cause of such discrepancies in $^{12}\text{C}/^{13}\text{C}$ and $^{12}\text{CO}/^{13}\text{CO}$ between our Galaxy and external galaxies is still unresolved. Here, we assumed an intermediate $^{12}\text{CO}/^{13}\text{CO}$ abundance ratio of 50 in NGC 2903 without any gradient across its disk for our LVG calculation. Note that we perform an additional LVG calculation for the center of NGC 2903 assuming the $^{12}\text{CO}/^{13}\text{CO}$ abundance ratios of 30 and 70 to evaluate the effect of the variation in the assumed $^{12}\text{CO}/^{13}\text{CO}$ abundance ratio on results of LVG calculation.

Figure 10 shows results of LVG calculation for each region in NGC 2903. The thin line indicates a curve of constant $R_{2-1/1-0}$ as functions of n_{H_2} and T_{K} , and the thick line indicates that of constant $R_{13/12}$. We can determine both n_{H_2} and T_{K} at the point where two curves intersect each other. Under the assumption of $^{12}\text{CO}/^{13}\text{CO}$ abundance ratio of 50, the derived n_{H_2} ranges from ~ 1000 cm^{-3} (in the disk; i.e., bar, bar-ends, and spiral arms) to 3700 cm^{-3} (at the center) and the derived T_{K} ranges from 10 K (in spiral arms) to 30 K (at the center). Note that both n_{H_2} and T_{K} vary depending on the assumption of $^{12}\text{CO}/^{13}\text{CO}$ abundance ratio; at the center of NGC 2903, the abundance ratio of 30 yields lower n_{H_2} of 1800 cm^{-3} and higher T_{K} of 38 K, whereas the abundance ratio of 70 yields higher n_{H_2} of 5900 cm^{-3} and intermediate T_{K} of 29 K. It seems that n_{H_2} is proportional to $^{12}\text{CO}/^{13}\text{CO}$ abundance ratio. This trend of n_{H_2} can be naturally explained if we consider the optical depth of ^{12}CO and ^{13}CO emission. ^{12}CO is always optically thick and thus its emission emerges from the diffuse envelope of dense gas clouds, while ^{13}CO emission emerges from further within these dense gas clouds due to its lower abundance. Since the increase in the assumed $^{12}\text{CO}/^{13}\text{CO}$ abundance ratio means that ^{13}CO becomes more optically thin, ^{13}CO emission emerged from deeper within the dense gas clouds and thus it probes denser gas. Derived physical properties, n_{H_2} and T_{K} , are summarized in table 3.

We compare the derived n_{H_2} and T_{K} in NGC 2903 with those determined in other external galaxies. Muraoka et al. (2012) determined n_{H_2} and T_{K} for GMCs associated with the giant H II region NGC 604 in M 33 at a spatial resolution of 100 pc using three molecular lines, $^{12}\text{CO}(J = 1 - 0)$, $^{13}\text{CO}(J = 1 - 0)$, and $^{12}\text{CO}(J = 3 - 2)$, based on the LVG approximation. The derived n_{H_2} and T_{K} are $800 - 2500$ cm^{-3} and 20 – 30 K, respectively, which are similar to our study for NGC 2903 in spite of the difference in the spatial resolution.

However, Schinnerer et al. (2010) obtained different physical properties for GMCs in spiral arms of M 51. They performed the LVG analysis using $R_{13/12}$ and $R_{2-1/1-0}$ at a spatial resolution of 120 – 180 pc. For the case of constant $dv/dr = 1.0 \text{ km s}^{-1} \text{ pc}^{-1}$, the derived T_K ranges from 10 to 50 K, which is similar to our study for NGC 2903, whereas n_{H_2} ranges from 100 to 400 cm^{-3} , which is 5 – 10 times lower than that in the disk of NGC 2903 in spite that the values of $R_{2-1/1-0}$ and $R_{13/12}$ in M 51 are not so different from those in NGC 2903. This is presumably due to the differences in assumed $Z(^{12}\text{CO})$ and $[^{12}\text{CO}]/[^{13}\text{CO}]$ abundance ratio. The authors assumed $Z(^{12}\text{CO})$ of 8.0×10^{-5} , which is higher than that assumed in our study, and a lower $[^{12}\text{CO}]/[^{13}\text{CO}]$ abundance ratio of 30. Under the LVG approximation with the assumption of $Z(^{12}\text{CO})$ of 8.0×10^{-5} , we found that the derived n_{H_2} is typically ~ 3 times lower than that with assumption of $Z(^{12}\text{CO})$ of 1.0×10^{-5} . Physically, high $Z(^{12}\text{CO})$ means abundant ^{12}CO molecules among molecular gas. In this condition, the optical depth of ^{12}CO line also increases, and thus the photon-trapping effect in molecular clouds becomes effective. Since this effect contributes the excitation of ^{12}CO molecule, an effective critical density of ^{12}CO line decreases. In other words, since the ^{12}CO is easily excited to upper J levels even in low molecular gas density, n_{H_2} at a given $R_{2-1/1-0}$ decreases. As a result, LVG analysis with the assumption of $Z(^{12}\text{CO})$ of 8.0×10^{-5} yields lower n_{H_2} . In addition, the low $[^{12}\text{CO}]/[^{13}\text{CO}]$ abundance ratio of 30 causes the decrease in the derived molecular gas density as described above. Therefore, the difference in the derived n_{H_2} between NGC 2903 and M 51 can be explained by the difference in the assumed $Z(^{12}\text{CO})$ and the $[^{12}\text{CO}]/[^{13}\text{CO}]$ abundance ratio.

4.2.2 Comparison of SFE with density and kinetic temperature of molecular gas

As described in section 1, SFEs often differ between galaxy centers and disks. Since NGC 2903 has a bright star forming region at the center, its SFE is expected to be higher than those in other regions. Here, we calculate SFEs for seven regions where averaged physical properties of molecular gas are obtained, and compare SFE with n_{H_2} and T_K in each region to examine what parameter controls SFE in galaxies.

SFE is expressed using the surface density of SFR (Σ_{SFR}) and that of molecular hydrogen (Σ_{H_2}) as follows:

$$\left[\frac{\text{SFE}}{\text{yr}^{-1}} \right] = \left(\frac{\Sigma_{\text{SFR}}}{M_{\odot} \text{ yr}^{-1} \text{ pc}^{-2}} \right) / \left(\frac{\Sigma_{\text{H}_2}}{M_{\odot} \text{ pc}^{-2}} \right) \quad (1)$$

We calculated extinction-corrected SFRs from a linear combination of $\text{H}\alpha$ and *Spitzer*/*MIPS* 24 μm luminosities using a following formula (Kennicutt 1998a; Kennicutt 1998b; Calzetti et al. 2007):

$$\Sigma_{\text{SFR}} = 7.9 \times 10^{-42} \left(\frac{L_{\text{H}\alpha} + 0.031 \times L_{24\mu\text{m}}}{\text{erg s}^{-1}} \right) \frac{\cos i}{\Omega} M_{\odot} \text{ yr}^{-1} \text{ pc}^{-2}, \quad (2)$$

where $L_{\text{H}\alpha}$ and $L_{24\mu\text{m}}$ mean $\text{H}\alpha$ and 24 μm luminosities, respectively. i is the inclination of 65°

for NGC 2903 and Ω is the covered area for each region (in the unit of pc^2). We used archival continuum-subtracted $\text{H}\alpha$ and $24\ \mu\text{m}$ images of NGC 2903 obtained by Hoopes et al. (2001) and the Local Volume Legacy survey project (Kennicutt et al. 2008; Dale et al. 2009), respectively. In addition, we calculated Σ_{H_2} using $I_{12\text{CO}(1-0)}$ as follows:

$$\left[\frac{\Sigma_{\text{H}_2}}{M_\odot \text{pc}^{-2}} \right] = 2.89 \times \cos i \left(\frac{I_{12\text{CO}(1-0)}}{\text{K km s}^{-1}} \right) \times \left\{ \frac{X_{\text{CO}}}{1.8 \times 10^{20} \text{cm}^{-2} (\text{K km s}^{-1})^{-1}} \right\}. \quad (3)$$

Here, we adopted a constant X_{CO} value of $1.8 \times 10^{20} \text{cm}^{-2} (\text{K km s}^{-1})^{-1}$ (Dame et al. 2001). We found that SFE at the center, $6.8 \times 10^{-9} \text{yr}^{-1}$, is 2 – 4 times higher than those in other regions. Calculated SFEs are listed in table 3.

We examined the dependence of SFE on n_{H_2} and T_{K} as shown in figure 11. We found that SFE positively correlates with both n_{H_2} and T_{K} . However, the trend of these correlations might change because it is possible that variations in the $^{12}\text{CO}/^{13}\text{CO}$ abundance ratio and X_{CO} affect the estimate of n_{H_2} , T_{K} , and SFE. In fact, both the $^{12}\text{CO}/^{13}\text{CO}$ abundance ratio and X_{CO} often differ between galaxy centers and disks. Therefore, we examine how variations in the $^{12}\text{CO}/^{13}\text{CO}$ abundance ratio and X_{CO} alter the estimate of n_{H_2} , T_{K} , and SFE at the center of NGC 2903.

We first consider the effect of the variation in $^{12}\text{CO}/^{13}\text{CO}$ abundance ratio on the estimate of n_{H_2} and T_{K} . As described in section 4.2.1, it is reported that the $^{12}\text{C}/^{13}\text{C}$ abundance ratio in our Galaxy increases with the galactocentric radius (Langer & Penzias 1990). Thus we examine the case of the lower $^{12}\text{CO}/^{13}\text{CO}$ abundance ratio at the center of NGC 2903. If we adopt the $^{12}\text{CO}/^{13}\text{CO}$ abundance ratio of 30 at the center, n_{H_2} and T_{K} are estimated to be 1800cm^{-3} and 38 K, respectively. This n_{H_2} value is slightly lower than that in the northern arm, whereas the positive correlation between SFE and n_{H_2} is not destroyed. Similarly, the T_{K} of 38 K does not destroy the positive correlation between SFE and T_{K} .

Next, we consider the effect of the variation in X_{CO} on the estimate of SFE. In central regions of disk galaxies, X_{CO} drops (i.e., CO emission becomes luminous at a given gas mass) by a factor of 2 – 3 or more (e.g., Nakai & Kuno 1995; Regan 2000), including the Galactic Center (e.g., Oka et al. 1998; Dahmen et al. 1998). Such a trend is presumably applicable to NGC 2903 considering the relationship between X_{CO} and metallicity, $12 + \log(\text{O}/\text{H})$. In general, X_{CO} decreases with the increase in metallicity because the CO abundance should be proportional to the carbon and oxygen abundances (e.g., Arimoto et al. 1996; Boselli et al. 2002). In addition, it is reported that metallicity decreases with the galactocentric distance in NGC 2903 (e.g., Dack & McCall 2012; Pilyugin et al. 2014). These observational facts suggest a smaller X_{CO} by a factor of 1.5 – 2 at the center than in the disk of NGC 2903, which yields a smaller gas mass, providing a higher SFE than the present one shown in table 3 and figure 11. However, even if a higher SFE by a factor of 2 is adopted for

the center, the global trend of the correlations shown in figure 11 does not change so much because the original SFE at the center is already the highest in NGC 2903. Therefore, we concluded that variations in the $^{12}\text{CO}/^{13}\text{CO}$ abundance ratio and X_{CO} do *not* affect the correlations of SFE with n_{H_2} and T_{K} in NGC 2903.

Note that the smaller X_{CO} corresponds to the larger $Z(^{12}\text{CO})$ at the center of NGC 2903, but the larger dv/dr is also suggested because the typical velocity width at the center ($250 - 300 \text{ km s}^{-1}$) is wider than those in other regions ($150 - 200 \text{ km s}^{-1}$) due to the rapid rotation of molecular gas near the galaxy center. Thus we consider that $Z(^{12}\text{CO})/(dv/dr)$ itself does not differ between the center and the disk in NGC 2903 even if the $Z(^{12}\text{CO})$ at the center is larger than that in the disk.

Finally, we examine the correlation coefficient for the least-square power-law fit R^2 between SFE and n_{H_2} and that between SFE and T_{K} shown in figure 11. We found that the former is 0.50 and the latter is 0.08. The significant correlation between SFE and n_{H_2} with R^2 of 0.50 suggests that molecular gas density governs the spatial variations in SFE. This speculation is well consistent with earlier studies based on HCN emission (e.g., Gao & Solomon 2004; Gao et al. 2007; Muraoka et al. 2009; Usero et al. 2015). In order to confirm whether such a relationship between SFE and n_{H_2} is applicable to other galaxies or not, we will perform further analysis toward other COMING sample galaxies, considering variations in the $^{12}\text{CO}/^{13}\text{CO}$ abundance ratio, X_{CO} , and $Z(^{12}\text{CO})/(dv/dr)$, in forthcoming papers.

5 Summary

We have performed the simultaneous mappings of $J = 1 - 0$ emission of ^{12}CO , ^{13}CO , and C^{18}O molecules toward the whole disk ($8' \times 5'$ or $20.8 \times 13.0 \text{ kpc}$ at the distance of 8.9 Mpc) of the nearby barred spiral galaxy NGC 2903 with the NRO 45-m telescope equipped with the FOREST at an effective angular resolution of $20''$ (or 870 pc). A summary of this work is as follows.

1. We detected $^{12}\text{CO}(J = 1 - 0)$ emission over the disk of NGC 2903. In addition, significant $^{13}\text{CO}(J = 1 - 0)$ emission was found at the center and bar-ends, whereas we could not detect any significant $\text{C}^{18}\text{O}(J = 1 - 0)$ emission.
2. In order to improve the S/N of CO emission and to measure $R_{2-1/1-0}$ and $R_{13/12}$ with high significance, we performed the stacking analysis for our $^{12}\text{CO}(J = 1 - 0)$, $^{13}\text{CO}(J = 1 - 0)$, and archival $^{12}\text{CO}(J = 2 - 1)$ spectra with velocity-axis alignment in nine representative regions (i.e., center, northern bar, southern bar, northern bar-end, southern bar-end, northern arm, southern arm, inter-arm, and outer-disk) of NGC 2903. We successfully obtained the stacked CO spectra with highly improved S/N, and thus we could confirm the significant $^{13}\text{CO}(J = 1 - 0)$ emission for all

Table 1. General parameters of NGC 2903

Morphological type ^a	SAB(rs)bc
Map center ^b :	
Right Ascension (J2000.0)	09 ^h 32 ^m 10 ^s .1
Declination (J2000.0)	21°30′03″.0
Distance ^c	8.9 Mpc
Linear scale	43 pc arcsec ⁻¹
Inclination ^d	65°

^aMorphological type from RC3. ^bMap center from Jarrett et al. (2003).

^cAdopted distance from Drozdovsky & Karachentsev (2000). ^dInclination from de Blok et al. (2008).

the regions.

3. We examined the averaged $R_{2-1/1-0}$ and $R_{13/12}$ for nine regions, and found that the averaged $R_{2-1/1-0}$ shows the highest value of 0.92 at the center, and moderate or lower values of 0.6 – 0.8 are observed in the disk. However, the highest $R_{13/12}$ of 0.19 is observed not at the center but in the northern arm. The central $R_{13/12}$ of 0.11 is similar to those in other regions (0.08 – 0.13) except for the northern arm and outer-disk (~ 0.04).
4. We determined n_{H_2} and T_{K} of molecular gas using $R_{2-1/1-0}$ and $R_{13/12}$ based on the LVG approximation. Under the assumption of $[^{12}\text{CO}]/[^{13}\text{CO}]$ abundance ratio of 50, the derived n_{H_2} ranges from $\sim 1000 \text{ cm}^{-3}$ (in the bar, bar-ends, and spiral arms) to 3700 cm^{-3} (at the center) and the derived T_{K} ranges from 10 K (in the bar and spiral arms) to 30 K (at the center).
5. We examined the dependence of SFE on n_{H_2} and T_{K} of molecular gas, and found the positive correlation between SFE and n_{H_2} with the correlation coefficient for the least-square power-law fit R^2 of 0.50. This suggests that molecular gas density governs the spatial variations in SFE.

We thank the referee for invaluable comments, which significantly improved the manuscript. We are indebted to the NRO staff for the commissioning and operation of the 45-m telescope and their continuous efforts to improve the performance of the instruments. This work is based on observations at NRO, which is a branch of the National Astronomical Observatory of Japan, National Institutes of Natural Sciences. This research has made use of the NASA/IPAC Extragalactic Database, which is operated by the Jet Propulsion Laboratory, California Institute of Technology, under contract with the National Aeronautics and Space Administration.

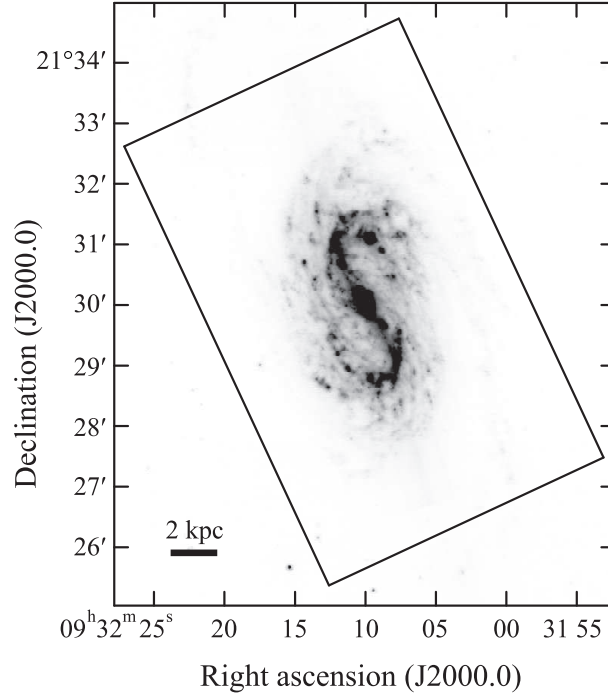


Fig. 1. Observed $8' \times 5'$ area of NGC 2903 with the FOREST mounted on the NRO 45-m telescope, which is indicated by a large square, superposed on *Spitzer*/IRAC $8 \mu\text{m}$ image (Kennicutt et al. 2008).

Table 2. Averaged line intensity and line ratios based on the stacking analysis

	$I_{12\text{CO}(1-0)}$ [K km s $^{-1}$]	$I_{12\text{CO}(2-1)}$ [K km s $^{-1}$]	$I_{13\text{CO}(1-0)}$ [K km s $^{-1}$]	$R_{2-1/1-0}$	$R_{13/12}$
Center	46.7 ± 0.7	43.0 ± 0.1	5.1 ± 0.2	0.92 ± 0.02	0.11 ± 0.01
Northern bar	26.4 ± 0.8	15.6 ± 0.1	2.2 ± 0.6	0.59 ± 0.02	0.08 ± 0.02
Southern bar	26.6 ± 0.8	18.1 ± 0.1	3.5 ± 0.7	0.68 ± 0.02	0.13 ± 0.03
Northern bar-end	36.8 ± 0.8	27.3 ± 0.1	3.6 ± 0.6	0.74 ± 0.02	0.10 ± 0.02
Southern bar-end	28.6 ± 0.6	21.2 ± 0.1	2.4 ± 0.6	0.74 ± 0.02	0.08 ± 0.02
Northern arm	19.8 ± 0.5	15.0 ± 0.1	3.8 ± 0.6	0.76 ± 0.02	0.19 ± 0.02
Southern arm	19.6 ± 0.5	11.9 ± 0.1	2.4 ± 0.4	0.61 ± 0.02	0.12 ± 0.02
Inter-arm	11.8 ± 0.3	7.2 ± 0.1	1.2 ± 0.3	0.61 ± 0.02	0.10 ± 0.02
Outer-disk	5.0 ± 0.2	3.2 ± 0.1	0.2 ± 0.1	0.64 ± 0.02	0.04 ± 0.02

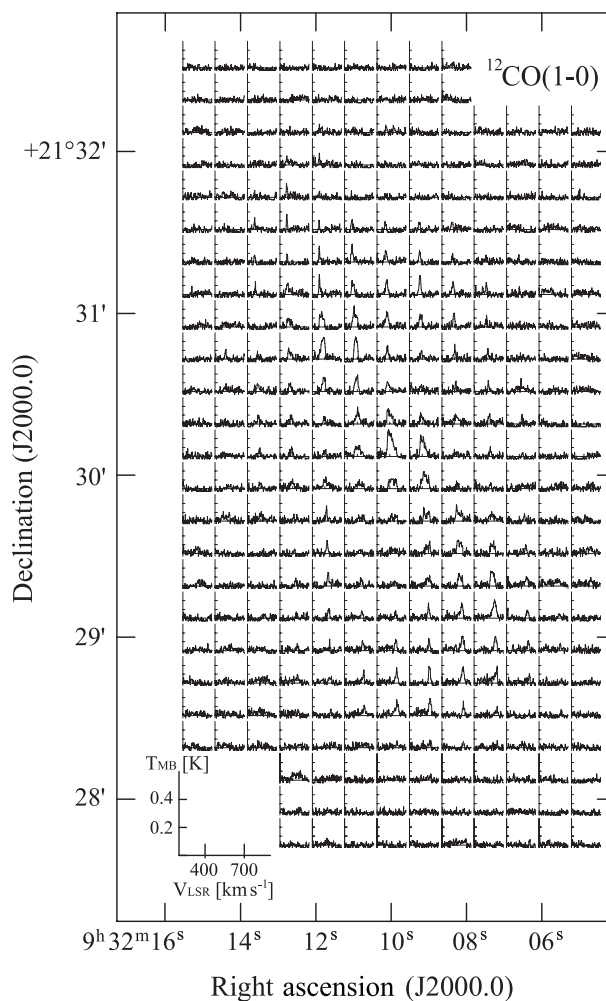


Fig. 2. Global spectra of $^{12}\text{CO}(J = 1 - 0)$ emission in NGC 2903. The grid spacing was set to $12''$ in order to display the spectrum in each pixel clearly. The temperature scale of spectra is indicated by the small box inserted in the lower left corner.

References

- Alonso-Herrero, A., Ryder, S. D., & Knapen, J. H. 2001, *MNRAS*, 322, 757
- Arimoto, N., Sofue, Y., & Tsujimoto, T. 1996, *PASJ*, 48, 275
- Bigiel, F., Leroy, A. K., Jiménez-Donaire, M. J., et al. 2016, *ApJL*, 822, L26
- Boselli, A., Lequeux, J., & Gavazzi, G. 2002, *A&A*, 384, 33
- Braine, J., Combes, F., Casoli, F., et al. 1993, *A&AS*, 97, 887
- Caldú-Primo, A., Schruba, A., Walter, F., et al. 2015, *AJ*, 149, 76
- Calzetti, D., et al. 2007, *ApJ*, 666, 870
- Chen, H., Gao, Y., Braine, J., & Gu, Q. 2015, *ApJ*, 810, 140
- Dack, S., & McCall, M. L. 2012, *ApJ*, 750, 167
- Dale, D. A., Cohen, S. A., Johnson, L. C., et al. 2009, *ApJ*, 703, 517

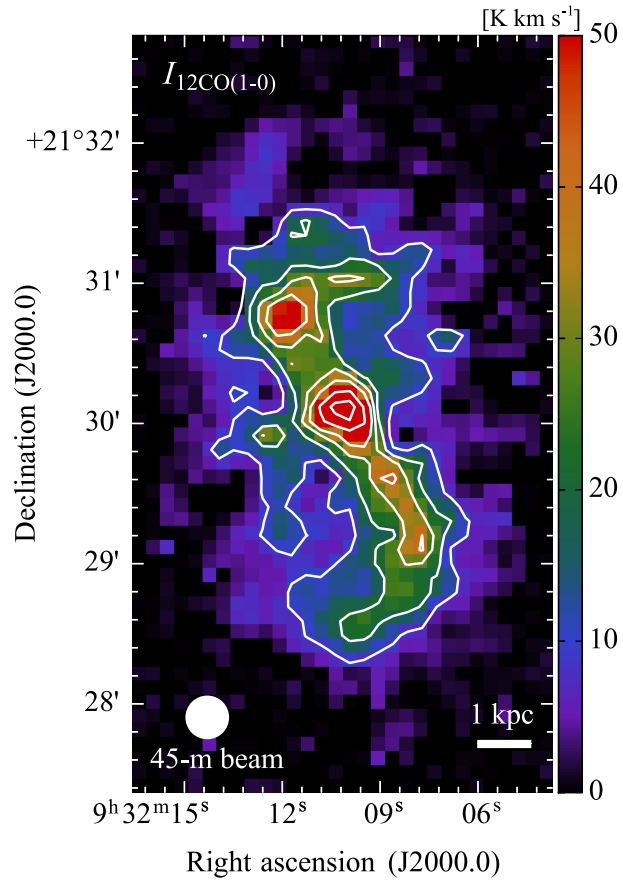


Fig. 3. A map of $I_{12\text{CO}(1-0)}$ of NGC 2903 obtained by COMING. The contour levels are 10, 20, 30, 40, 60, and 80 K km s^{-1} .

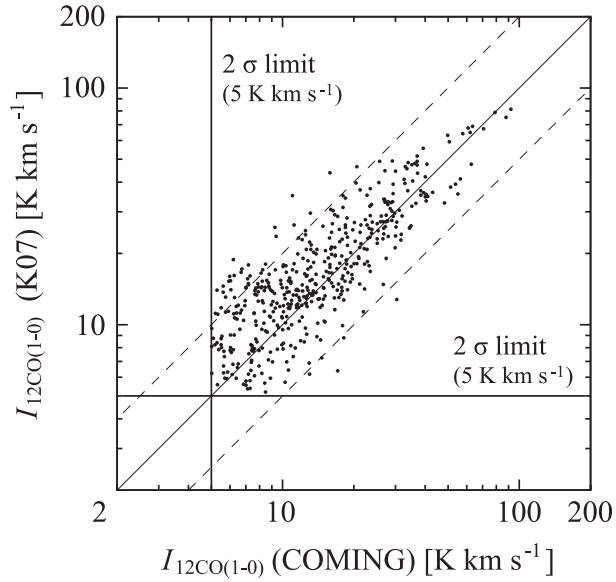


Fig. 4. A pixel-by-pixel comparison between $I_{12\text{CO}(1-0)}$ in NGC 2903 obtained by COMING and those obtained by K07. The vertical and horizontal lines indicate the 2σ of $I_{12\text{CO}(1-0)}$ for COMING and K07 data, respectively. The diagonal solid line indicates the ratio of $I_{12\text{CO}(1-0)}$ by COMING to those by K07 of unity, and the dashed lines indicate the ratio of 0.5 and 2.0. Both $I_{12\text{CO}(1-0)}$ are well correlated with each other.

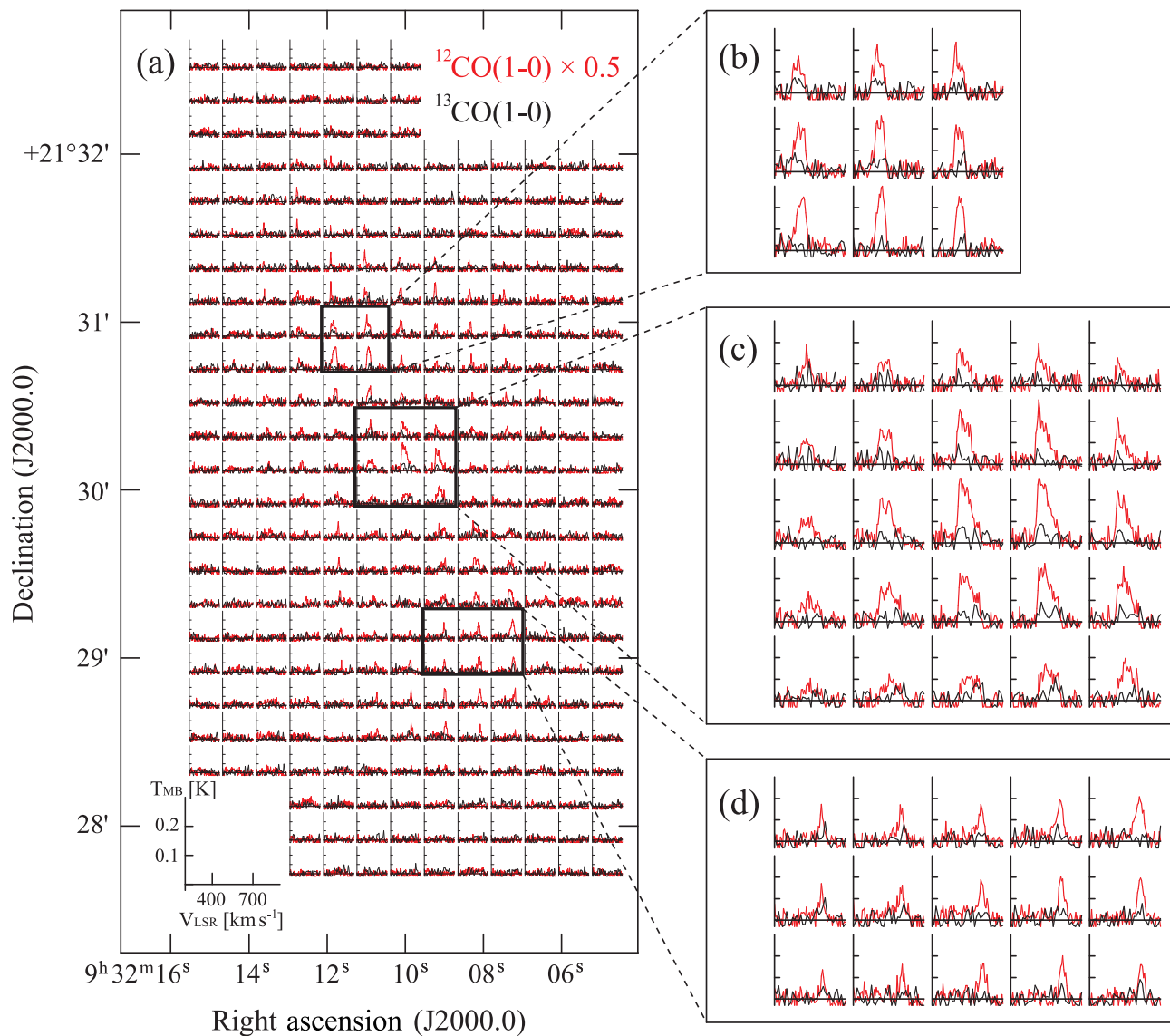


Fig. 5. (a) Global spectra of $^{13}\text{CO}(J=1-0)$ emission in NGC 2903. For comparison, spectra of $^{12}\text{CO}(J=1-0)$ emission multiplied by 0.5 are overlaid in red line. As well as figure 2, the grid spacing was set to $12''$. The temperature scale of spectra is indicated by the small box inserted in the lower left corner. (b) Magnified spectra with the grid spacing of $6''$ at the northern bar-end. (c) Same as (b), but at the center. (d) Same as (b), but at the southern bar-end.

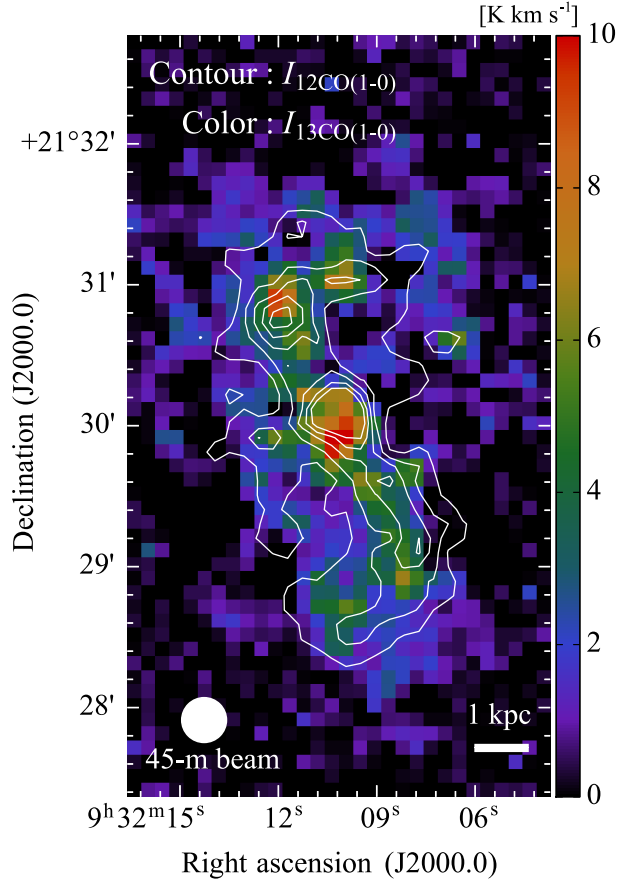


Fig. 6. A color map of $I_{13\text{CO}(1-0)}$ superposed on the contour map of $I_{12\text{CO}(1-0)}$ of NGC 2903. The contour levels of $I_{12\text{CO}(1-0)}$ are the same as figure 3.

Table 3. Derived n_{H_2} and T_{K} , and SFE in each region of NGC 2903

region	$^{12}\text{CO}/^{13}\text{CO}$	n_{H_2} [10^3 cm^{-3}]	T_{K} [K]	SFE [10^9 yr^{-1}]
Center	50	$3.7^{+1.2}_{-0.9}$	30 ± 3	6.8 ± 0.8
Northern bar	50	$0.96^{+0.22}_{-0.28}$	14^{+5}_{-4}	3.2 ± 0.4
Southern bar	50	$1.5^{+0.2}_{-0.3}$	12^{+4}_{-3}	2.0 ± 0.3
Northern bar-end	50	1.4 ± 0.2	18^{+4}_{-3}	1.6 ± 0.2
Southern bar-end	50	1.2 ± 0.3	20^{+10}_{-4}	1.5 ± 0.2
Northern arm	50	$2.1^{+0.4}_{-0.3}$	12 ± 3	3.6 ± 0.5
Southern arm	50	1.3 ± 0.2	10^{+3}_{-2}	2.8 ± 0.4
Center	30	$1.8^{+0.4}_{-0.2}$	38 ± 3	6.8 ± 0.8
Center	70	$5.9^{+3.9}_{-1.8}$	29^{+5}_{-4}	6.8 ± 0.8

$^{12}\text{CO}/^{13}\text{CO}$ means the assumed $^{12}\text{CO}/^{13}\text{CO}$ abundance ratio for the LVG calculation.

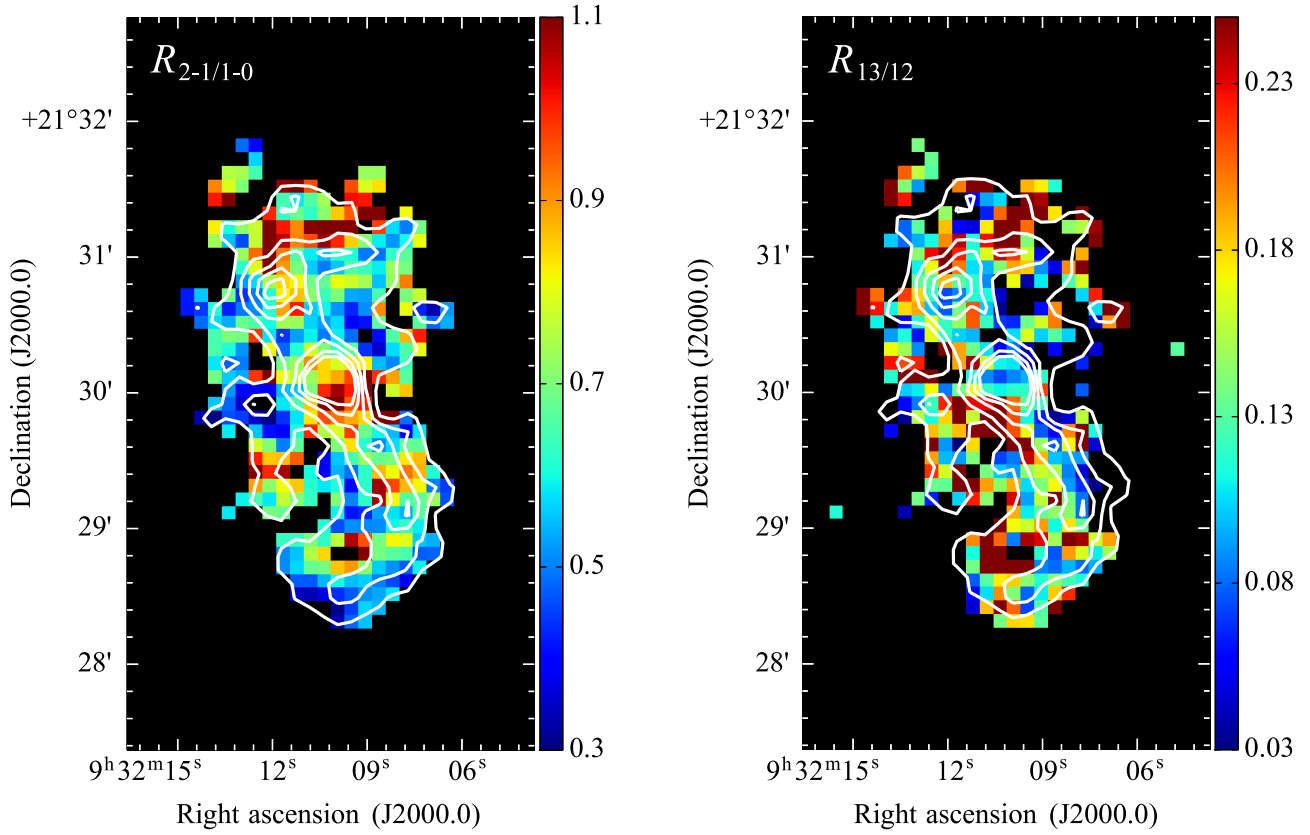


Fig. 7. Spatial distributions of $R_{2-1/1-0}$ (left) and $R_{13/12}$ (right) superposed on the contour map of $I_{12\text{CO}(1-0)}$ of NGC 2903. The contour levels of $I_{12\text{CO}(1-0)}$ are the same as figure 3. There are some local peaks of $R_{2-1/1-0}$ (~ 1.0) near the center and at the downstream side of the northern spiral arm, whereas lower $R_{2-1/1-0}$ ($\sim 0.5 - 0.6$) was observed in the bar. The spatial distribution of $R_{13/12}$ is unclear due to poor S/N of $^{13}\text{CO}(J = 1 - 0)$ emission.

- Dahmen, G., Huttemeister, S., Wilson, T. L., & Mauersberger, R. 1998, *A&A*, 331, 959
- Dame, T. M., Hartmann, D., & Thaddeus, P. 2001, *ApJ*, 547, 792
- de Blok, W. J. G., Walter, F., Brinks, E., et al. 2008, *AJ*, 136, 2648
- Drozdovsky, I. O., & Karachentsev, I. D. 2000, *A&AS*, 142, 425
- Elfhag, T., Booth, R. S., Hoeglund, B., Johansson, L. E. B., & Sandqvist, A. 1996, *A&AS*, 115, 439
- Emerson, D. T., & Graeve, R. 1988, *A&A*, 190, 353
- Gao, Y., Carilli, C. L., Solomon, P. M., & Vanden Bout, P. A. 2007, *ApJL*, 660, L93
- Gao, Y., & Solomon, P. M. 2004a, *ApJ*, 606, 271
- Goldreich, P., & Kwan, J. 1974, *ApJ*, 189, 441
- Helfer, T. T., Thornley, M. D., Regan, M. W., et al. 2003, *ApJS*, 145, 259
- Henkel, C., Chin, Y.-N., Mauersberger, R., & Whiteoak, J. B. 1998, *A&A*, 329, 443
- Henkel, C., Mauersberger, R., Wiklind, T., et al. 1993, *A&A*, 268, L17
- Henkel, C., Whiteoak, J. B., & Mauersberger, R. 1994, *A&A*, 284, 17

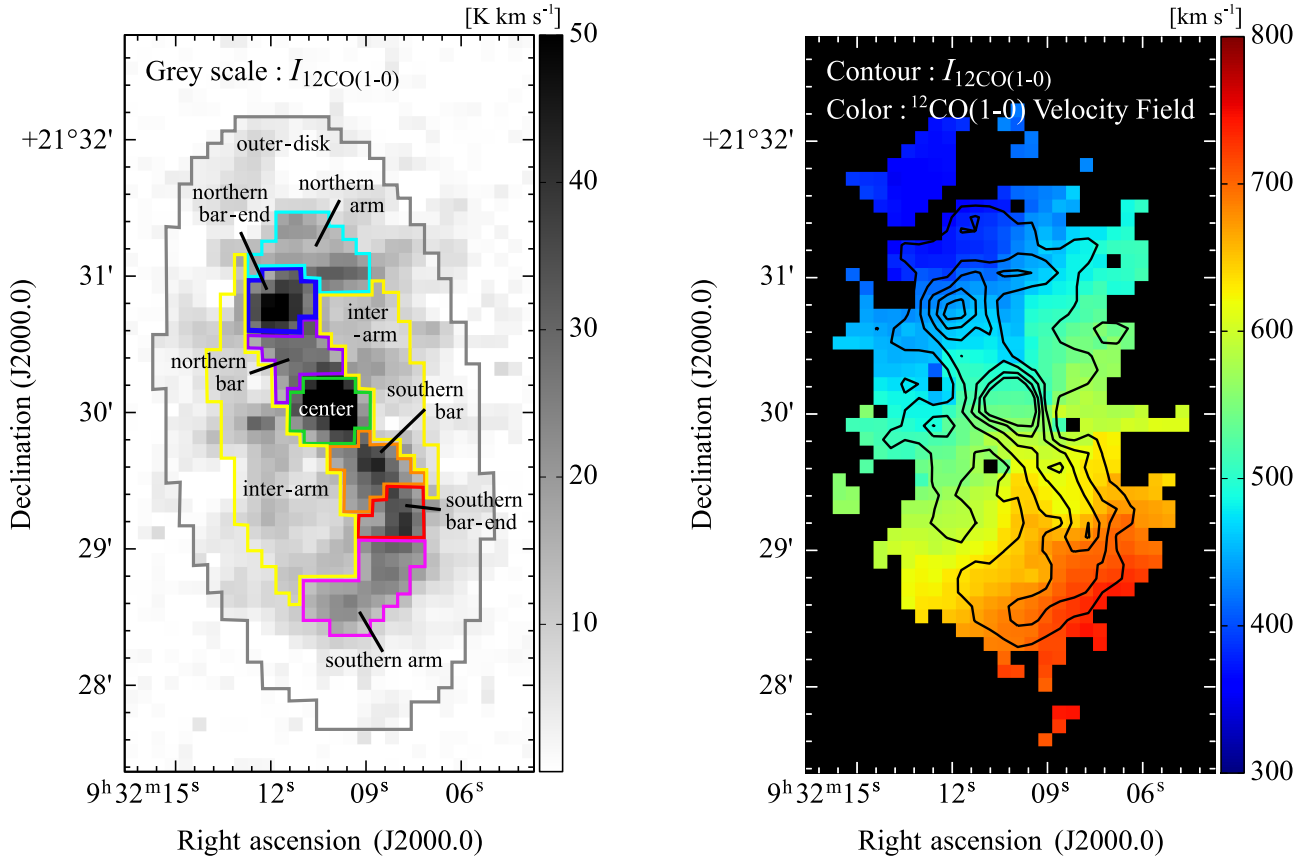


Fig. 8. (left) Separation of representative regions for stacking analysis superposed on the grey-scale map of $I_{12\text{CO}(1-0)}$ of NGC 2903. The green frame indicates the center, the purple and orange indicate the northern and southern bars, the blue and red indicate the northern and southern bar-ends, the cyan and magenta indicate the northern and southern arms, the yellow indicates the inter-arm, and the grey indicates the outer-disk. (right) Intensity-weighted mean velocity field calculated from $^{12}\text{CO}(J = 1 - 0)$ data superposed on the contour map of $I_{12\text{CO}(1-0)}$. The contour levels of $I_{12\text{CO}(1-0)}$ are the same as figure 3.

Hirota, A., Kuno, N., Sato, N., et al. 2010, PASJ, 62, 1261

Hoopes, C. G., Walterbos, R. A. M., & Bothun, G. D. 2001, ApJ, 559, 878

Jarrett, T. H., Chester, T., Cutri, R., Schneider, S. E., & Huchra, J. P. 2003, AJ, 125, 525

Kennicutt, R. C., Jr. 1998a, ApJ, 498, 541

Kennicutt, R. C., Jr. 1998b, ARA&A, 36, 189

Kennicutt, R. C., Jr., Lee, J. C., Funes, S. J., José G., Sakai, S., & Akiyama, S. 2008, ApJS, 178, 247

Kuno, N., Sato, N., Nakanishi, H., et al. 2007, PASJ, 59, 117

Langer, W. D., & Penzias, A. A. 1990, ApJ, 357, 477

Laurikainen, E., & Salo, H. 2002, MNRAS, 337, 1118

Leroy, A. K., Walter, F., Bigiel, F., et al. 2009, AJ, 137, 4670

Leroy, A. K., Walter, F., Sandstrom, K., et al. 2013, AJ, 146, 19

Mao, R. Q., Henkel, C., Schulz, A., et al. 2000, A&A, 358, 433

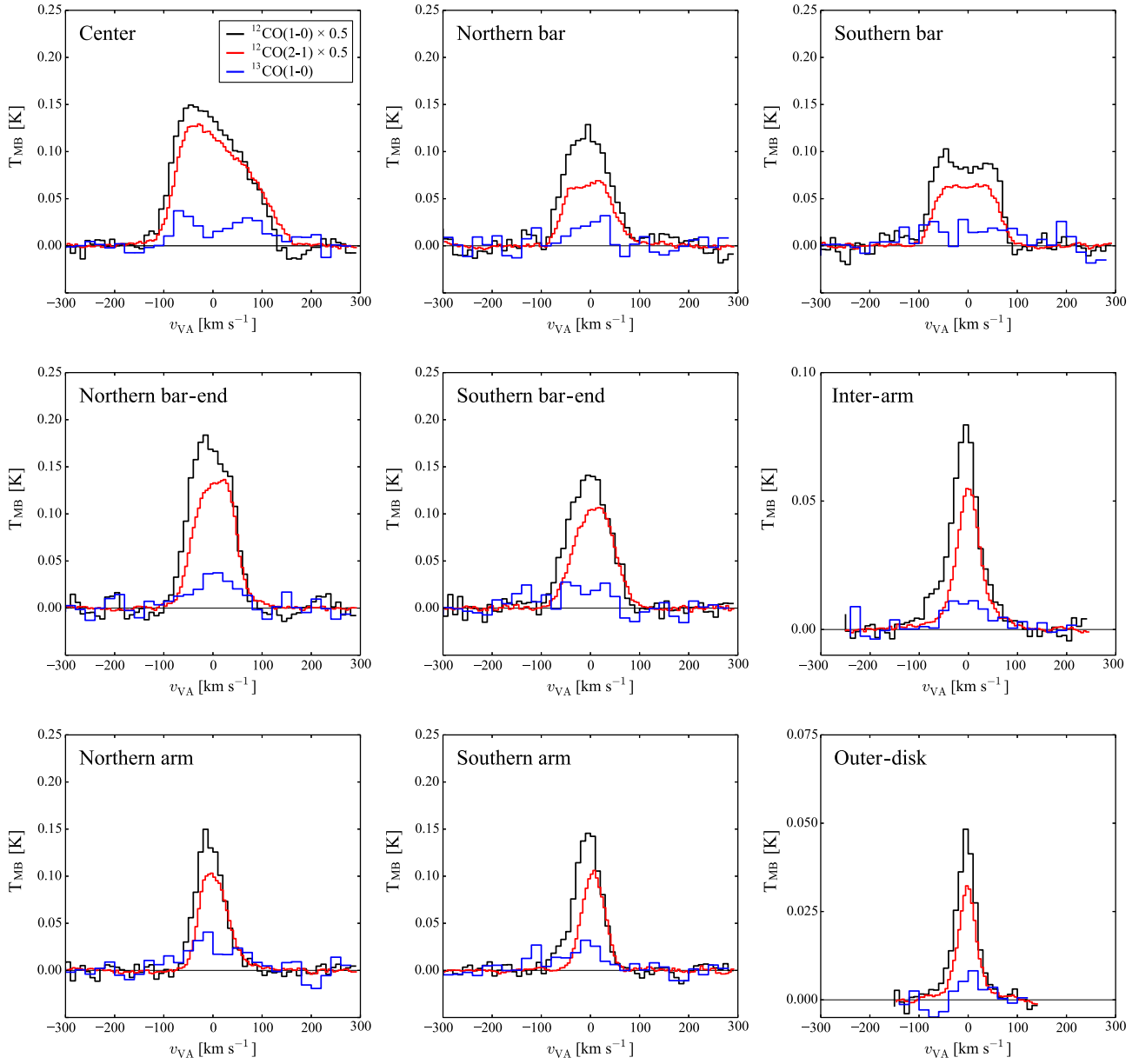


Fig. 9. Stacked CO spectra for each region in NGC 2903. The black line indicates $^{12}\text{CO}(J = 1 - 0)$ emission multiplied by 0.5, the red indicates $^{12}\text{CO}(J = 2 - 1)$ emission multiplied by 0.5, and the blue indicates $^{13}\text{CO}(J = 1 - 0)$ emission. The S/N of each CO emission is dramatically improved, and thus a significant $^{13}\text{CO}(J = 1 - 0)$ emission is confirmed for all the regions.

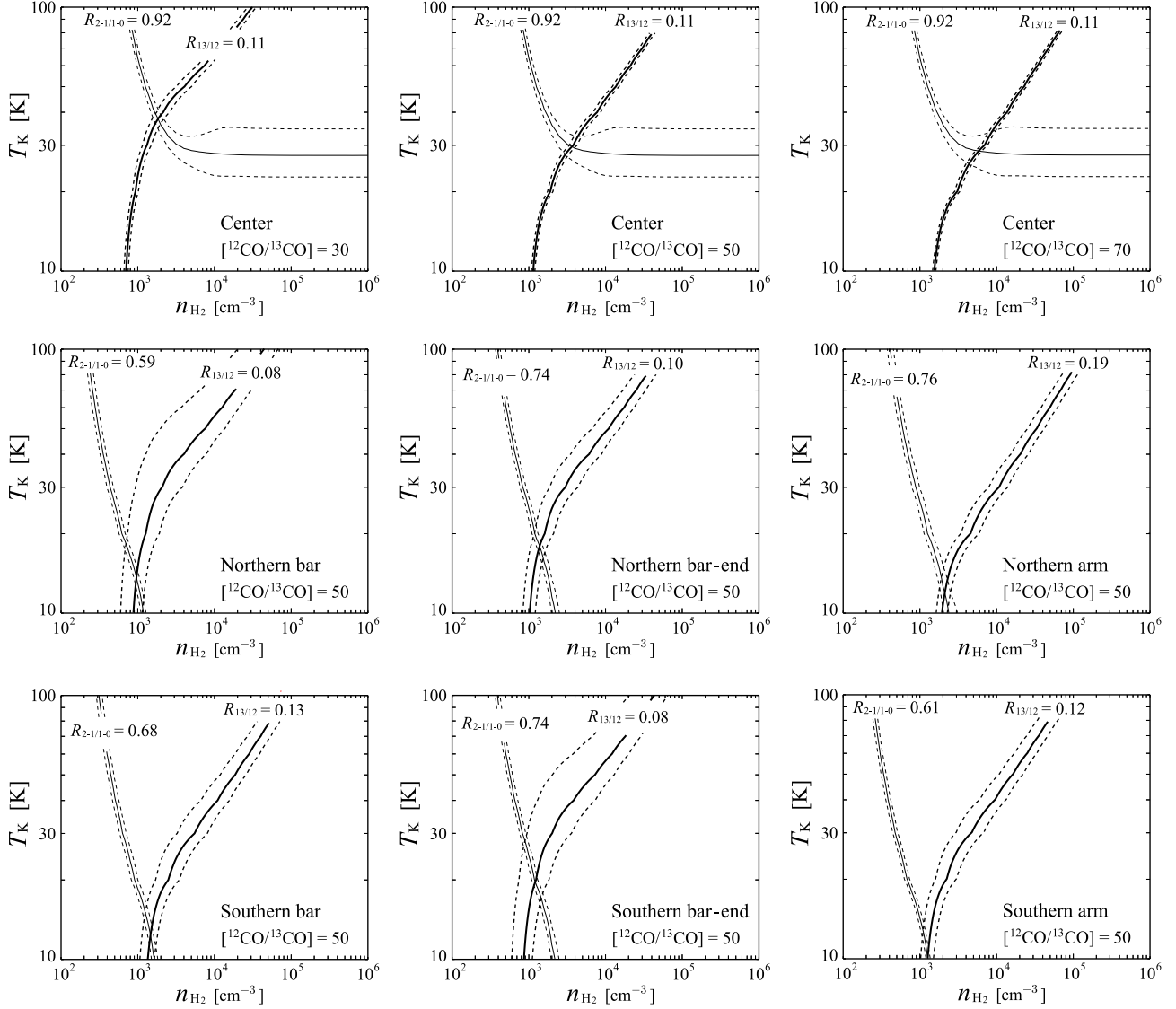


Fig. 10. Curves of constant $R_{2-1/1-0}$ (thin line) and $R_{13/12}$ (thick line) as functions of molecular gas density n_{H_2} and kinetic temperature T_{K} . ^{12}CO fractional abundance per unit velocity gradient $Z(^{12}\text{CO})/(dv/dr)$ was assumed to be $1.0 \times 10^{-5} (\text{km s}^{-1} \text{pc}^{-1})^{-1}$. The $[^{12}\text{CO}]/[^{13}\text{CO}]$ abundance ratio was assumed to be a fixed value of 50 for the bar, bar-ends, and spiral arms, but three different $[^{12}\text{CO}]/[^{13}\text{CO}]$ abundance ratios of 30, 50, and 70 were assumed for the center. Dashed lines indicate $\pm 1\sigma$ error of each line ratio.

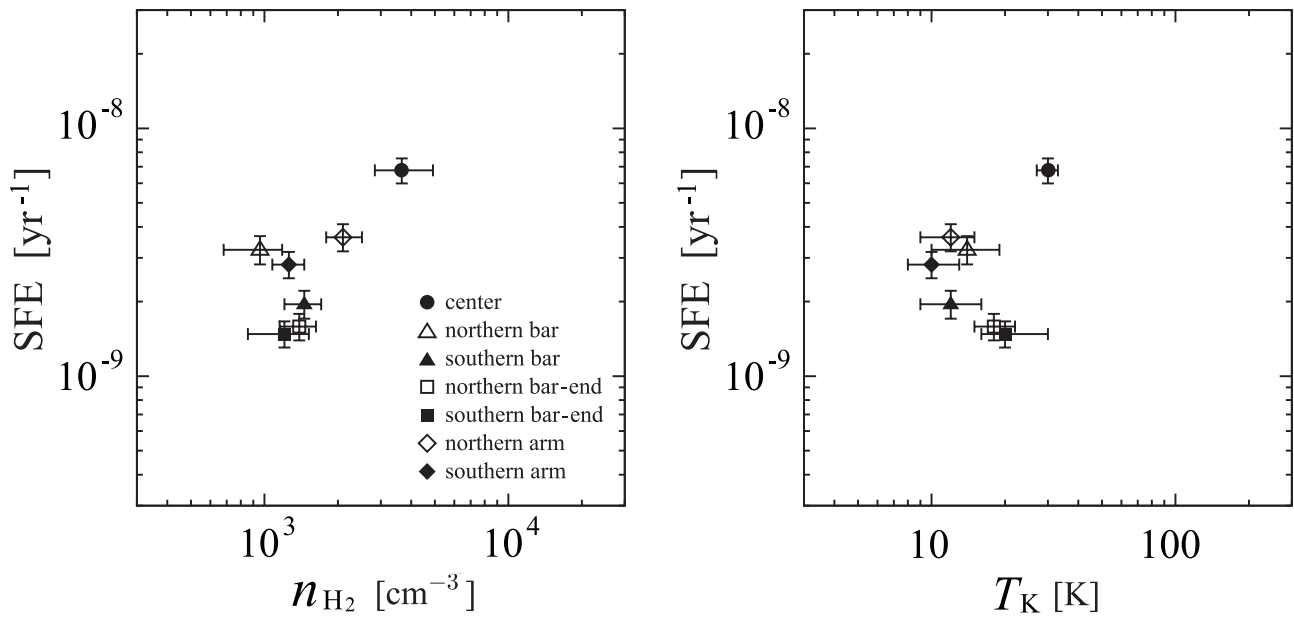


Fig. 11. Correlation between SFE and n_{H_2} (left) and that between SFE and T_{K} (right) in each region of NGC 2903.

Martín, S., Aladro, R., Martín-Pintado, J., & Mauersberger, R. 2010, A&A, 522, A62

Minamidani, T., Mizuno, N., Mizuno, Y., et al. 2008, ApJS, 175, 485

Minamidani, T., Nishimura, A., Miyamoto, Y., et al. 2016, Proc. SPIE, 9914, submitted

Morokuma-Matsui, K., Sorai, K., Watanabe, Y., & Kuno, N. 2015, PASJ, 67, 2

Muraoka, K., Kohno, K., Tosaki, T., et al. 2007, PASJ, 59, 43

Muraoka, K., Kohno, K., Tosaki, T., et al. 2009, PASJ, 61, 163

Muraoka, K., Tosaki, T., Miura, R., et al. 2012, PASJ, 64, 3

Nakai, N., & Kuno, N. 1995, PASJ, 47, 761

Nakajima, T., Kimura, K., Nishimura, A., et al. 2013, PASP, 125, 252

Oka, T., Hasegawa, T., Hayashi, M., Handa, T., & Sakamoto, S. 1998, ApJ, 493, 730

Paglione, T. A. D., Wall, W. F., Young, J. S., et al. 2001, ApJS, 135, 183

Pilyugin, L. S., Grebel, E. K., & Kniazev, A. Y. 2014, AJ, 147, 131

Regan, M. W. 2000, ApJ, 541, 142

Sawada, T., Ikeda, N., Sunada, K., et al. 2008, PASJ, 60, 445

Sakamoto, S., Handa, T., Sofue, Y., Honma, M., & Sorai, K. 1997, ApJ, 475, 134

Scoville, N. Z. & Solomon, P. M. 1974, ApJ, 187, L67

Schinnerer, E., Weiß, A., Aalto, S., & Scoville, N. Z. 2010, ApJ, 719, 1588

Schruba, A., Leroy, A. K., Walter, F., et al. 2011, AJ, 142, 37

Schruba, A., Leroy, A. K., Walter, F., et al. 2012, AJ, 143, 138

Simons, D. A., Depoy, D. L., Becklin, E. E., et al. 1988, ApJ, 335, 126

Sorai, K., Kuno, N., Nishiyama, K., et al. 2012, PASJ, 64, 51
Tosaki, T., Hasegawa, T., Shioya, Y., Kuno, N., & Matsushita, S. 2002, PASJ, 54, 209
Usero, A., Leroy, A. K., Walter, F., et al. 2015, AJ, 150, 115
Vila-Vilaro, B., Cepa, J., & Zabludoff, A. 2015, ApJS, 218, 28
Watanabe, Y., Sorai, K., Kuno, N., & Habe, A. 2011, MNRAS, 411, 1409
Wynn-Williams, C. G., & Becklin, E. E. 1985, ApJ, 290, 108
Young, J. S., Allen, L., Kenney, J. D. P., Lesser, A., & Rownd, B. 1996, AJ, 112, 1903
Young, J. S., Xie, S., Tacconi, L., et al. 1995, ApJS, 98, 219
Yukita, M., Swartz, D. A., Tennant, A. F., Soria, R., & Irwin, J. A. 2012, ApJ, 758, 105